Ionization potentials of (112) and (11$\bar{2}$) facet surfaces of $CuInSe_2$ and $CuGaSe_2$

Yoyo Hinuma,[1,*] Fumiyasu Oba,[1,†] Yu Kumagai,[1,2] and Isao Tanaka[1,3]
[1]*Department of Materials Science and Engineering, Kyoto University, Kyoto 606-8501, Japan*
[2]*Department of Materials, ETH Zurich, Zürich 8093, Switzerland*
[3]*Nanostructures Research Laboratory, Japan Fine Ceramics Center, Nagoya 456-8587, Japan*
(Received 6 October 2012; revised manuscript received 20 November 2012; published 26 December 2012)

The ionization potentials of the faceted and nonfaceted (110) surfaces of $CuInSe_2$ (CIS) and $CuGaSe_2$ (CGS), which are key components of $CuIn_{1-x}Ga_xSe_2$ (CIGS) thin-film solar cells, are investigated using first-principles calculations based on a hybrid Hartree-Fock density functional theory approach. Slab models of the chalcopyrite (110) surface with both (112) and (11$\bar{2}$) facets on each surface of the slab are employed. Surface energy evaluations point out that two types of faceted surfaces with point defects, namely a combination of Cu_{In} (Cu_{Ga}) and In_{Cu} (Ga_{Cu}) antisites and a combination of Cu vacancies and In_{Cu} (Ga_{Cu}) antisites, are the most stable depending on the chemical potentials. The ionization potentials are evaluated with two definitions: One highly sensitive to and the other less sensitive to localized surface states. The latter varies by 0.4 eV in CIS and 0.5 eV in CGS with the surface structure. The ionization potentials are reduced by 0.2 eV for faceted surfaces with Cu_{In} (Cu_{Ga}) and In_{Cu} (Ga_{Cu}) antisites when the effects of the localized surface states are considered. The values of both ionization potentials are similar between CIS and CGS with a difference of about 0.1 eV for the most stable surface structures.

DOI: 10.1103/PhysRevB.86.245433 PACS number(s): 73.20.At, 68.35.bg

I. INTRODUCTION

$CuInSe_2$ (CIS) and $CuGaSe_2$ (CGS) are key components of $CuIn_{1-x}Ga_xSe_2$ (CIGS) thin-film solar cells that utilize CIGS alloys as photoabsorbers.[1,2] The composition of the CIGS alloy is chosen to attain the optimum energy conversion efficiency, which is strongly influenced by the band gap. A typical cell structure consists of a *p*-type CIGS layer and an *n*-type such as CdS and Zn or In compounds. The atomic and electronic structure, local composition, and point defect formation at the heterojunctions are considered to play crucial roles in the determination of the cell efficiency. Knowledge on the microstructure and the atomic and electronic structures of the surfaces of CIS and CGS as well as of CIGS are fundamentally important because the interfacial properties of a cell can be affected by the surface structure of these films during fabrication.

CIS and CGS take the chalcopyrite structure (space group $I\bar{4}2d$) and have a nonpolar (110) surface that has been reported to further stabilize when facets consisting of polar (112) and (11$\bar{2}$) planes with defects form on this surface.[3,4] Jaffe and Zunger carried out first-principles calculations within the local density approximation (LDA) to density functional theory on individual (112) and (11$\bar{2}$) surfaces of CIS as well as the nonpolar (110) surface.[3] They suggested that the formation of Cu vacancies and Cu_{In} antisites stabilizes surface structures with (112) and (11$\bar{2}$) facets and makes the faceted surface lower in energy than the (110) surface under most chemical potential conditions; however, the electronic structure of these surfaces has not been reported.

In this study, the stability, electronic structure, and ionization potentials (IPs) of the faceted and nonfaceted (110) surfaces of CIS and CGS are investigated using first-principles calculations based on a hybrid Hartree-Fock density functional theory approach. We employ a faceted slab model of the chalcopyrite (110) surface that contains both (112) and (11$\bar{2}$) facets on each surface of the slab and therefore has zero net dipole moment. We particularly focus on the IP among surface properties because the IP of semiconductors and insulators is a measure of the position of the valence band with respect to the vacuum level, and therefore is a fundamental quantity in the understanding and control of catalytic and photocatalytic properties at the surface. The IP also provides an estimate of the interfacial band offsets at heterojunctions in solar cells as well as in electronic and optoelectronic devices, although the difference in the effects of dipoles at surfaces and interfaces needs to be considered for accurate discussion. Furthermore, band alignment diagrams based on the IPs provide useful information on the doping limit and interface design.[5] However, obtaining the IP is nontrivial because this quantity is directly affected by the dipole moment at the surface. In other words, the IP is a function of the surface orientation, composition, and defects. As a consequence, experimental determination is difficult for systems in which well-defined surface structures are not readily prepared, and therefore theoretical evaluation is effective.

We consider two quantities as the IP. The first quantity is defined as the difference between the vacuum level and the highest occupied level in the bulk region far from the surface. This is referred to as the bulk-based IP. The second is called the surface-sensitive IP and is taken as the difference between the vacuum level and the highest occupied level in a slab model. Particular electronic states may form in many cases in the vicinity of the surfaces, which can locally affect the valence states. The surface-sensitive IP would become relevant when we are interested in properties that may be influenced by localized surface states. In this study, these two quantities are evaluated for a variety of surfaces including faceted/nonfaceted and pristine/defective structures.

II. METHODOLOGY

The calculations are performed using the projector augmented wave (PAW) method[6] with the Heyd-Scuseria-Ernzerhof (HSE06) hybrid functional[7–9] as implemented in

 ©2012 American Physical Society

TABLE I. Calculated and experimental structural parameters (the lattice constants a and c and the internal parameter u) and band gap (E_g) for CIS.

	GGA + U	HSE06 ($a = 0.25$)	HSE06 ($a = 0.3$)	Experiment
a (Å)	5.878	5.845	5.837	5.784[a]
c (Å)	11.828	11.756	11.730	11.616[a]
u	0.221	0.225	0.227	0.224[a]
E_g (eV)	0.08	0.78	1.04	1.05[b]

[a]Reference 30.
[b]Reference 31.

the VASP code.[10–13] A plane-wave cutoff energy of 400 eV was used. The amount of Hartree-Fock exchange mixing in the HSE06 functional is increased from the standard value of 0.25 to 0.3 so as to better reproduce the band gaps of CIS and CGS.[14–16] This functional, noted as HSE06 ($a = 0.3$) hereafter, has been reported to provide similar results to those obtained by changing the screening parameter of the HSE06 functional from 0.208 to 0.13 Å^{-1}.[17] The faceted and nonfaceted (110) surfaces of CIS and CGS are treated using slab models. Γ-centered k meshes of $4 \times 2 \times 1$ and $4 \times 4 \times 1$ were used with faceted and nonfaceted (110) surface slab models, respectively. Spin polarization was allowed in all calculations. In the slab calculations, the atomic coordinates were obtained using the Hubbard U correction to the generalized gradient approximation (GGA + U) to density functional theory since atomic relaxation using the HSE06 ($a = 0.3$) functional is computationally too demanding. The Perdew-Burke-Ernzerhof functional[18] and Dudarev's approach[19] with $U - J = 5$ eV on Cu 3d orbitals were used in the GGA + U calculations. The in-plane lattice parameters were first fixed to GGA + U bulk values and the atomic coordinates were fully relaxed using GGA + U. The in-plane lattice parameters and the cell dimension in the out-of-plane (slab thickness) direction were then scaled to HSE06 ($a = 0.3$) bulk values with the fractional atomic coordinates fixed to the GGA + U values, and HSE06 ($a = 0.3$) calculations were conducted without relaxation of atomic coordinates. The lattice constants a and c, the internal parameters for the Se coordinates u, and the band gaps obtained by GGA + U and HSE06 for CIS and CGS are summarized in Tables I and II, respectively. GGA + U significantly underestimates the band gaps. In particular, the band gap of CIS is very small at around 0.1 eV,

TABLE II. Calculated and experimental structural parameters (the lattice constants a and c and the internal parameter u) and band gap (E_g) for CGS.

	GGA + U	HSE06 ($a = 0.25$)	HSE06 ($a = 0.3$)	Experiment
a (Å)	5.689	5.657	5.650	5.614[a]
c (Å)	11.225	11.125	11.088	11.030[a]
u	0.246	0.251	0.252	0.250[a]
E_g (eV)	0.50	1.33	1.62	1.68[b]

[a]Reference 30.
[b]Reference 32.

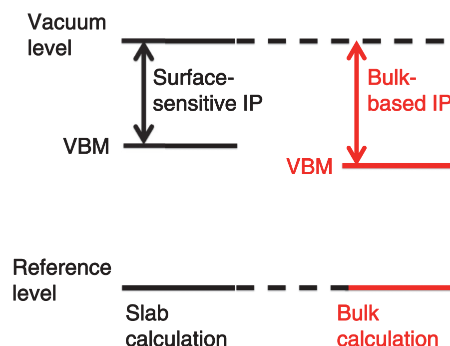

FIG. 1. (Color online) Schematic showing two methods to calculate the ionization potential (IP).

which makes it difficult to discuss in-gap electronic states at the surface. The values with the HSE06 ($a = 0.3$) functional, which is employed in this study except the relaxation of atomic coordinates, are closest to the experimental values not only in the band gaps but also in the lattice constants for both CIS and CGS.

Figure 1 shows two definitions of the IP considered in this work. The surface-sensitive IP is obtained from slab calculations only, where the difference between the vacuum level and the highest occupied level in a slab model is taken as the IP (black arrow in Fig. 1). The orbitals that contribute to the highest occupied state may primarily come from surface atoms, atoms at the center of the slab, or both. Therefore, this IP is strongly affected by surface states, if any, and this definition is adopted in a hybrid functional study of In_2O_3 surfaces by Walsh and Catlow.[20] On the other hand, the surface-sensitive IP should converge to the bulk-based IP when there are no occupied surface states in the band gap, and atoms at the center of the slab constitute the highest occupied level as discussed later. The bulk-based IP is derived using the difference between the vacuum level and a reference level in the region far from the surface in a slab model and the difference between the valence band maximum (VBM) and the reference level from a bulk model. This IP is taken as the difference between the vacuum level in the slab model and the VBM in the bulk model when the reference levels are aligned (red arrow in Fig. 1). Hohmann *et al.* used a similar definition of the IP in their work on In_2O_3 surfaces.[21] The geometry of the bulk model used to calculate the bulk-based IP is obtained in the same way as the surface model; the geometry optimization was performed with GGA + U and the lattice parameters were then scaled to the HSE06 ($a = 0.3$) values. Apart from the scaling of the cell dimensions, this approach is similar to that reported by Moses *et al.*, where the valence band position from HSE calculations using surface geometry optimized with PBE were shown to produce very good agreement with differences less than 0.05 eV compared to when the geometry was optimized with HSE in AlN, GaN, and InN.[22] The IPs are increased by 0.08 and 0.07 eV for CIS and CGS, respectively, when the bulk geometry optimized by HSE06 ($a = 0.3$) is used because of the change in the difference between the VBM and reference levels caused by the small atomic displacements. An electrostatic potential averaged within a PAW sphere at each atomic site was taken as a reference level, and the 1:1:2 averages of Cu, In (Ga), and

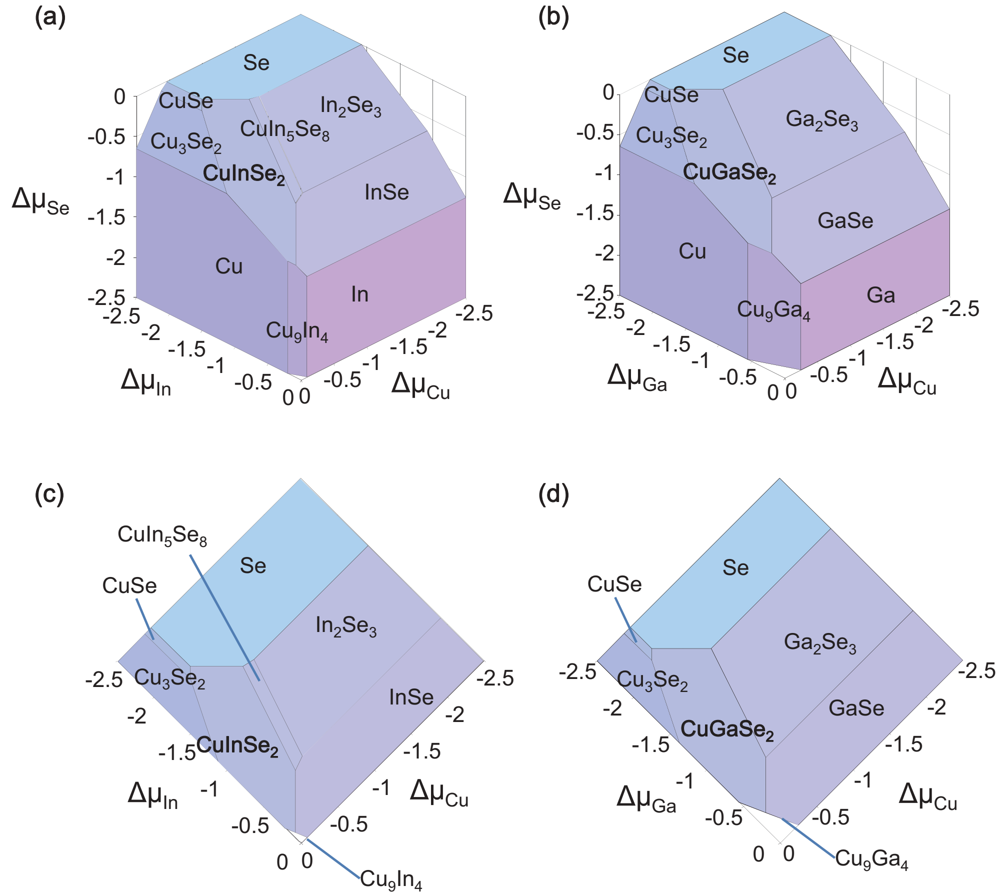

FIG. 2. (Color online) Chemical potential diagrams of (a) the Cu-In-Se and (b) Cu-Ga-Se systems showing stable phases under given chemical potentials. (c) The projection onto the $\Delta\mu_{Cu}$-$\Delta\mu_{In}$ plane and (d) the $\Delta\mu_{Cu}$-$\Delta\mu_{Ga}$ plane. Chemical potentials are shown in eV.

Se atoms were considered. The vacuum level was determined by the local potential in the vacuum region of the slab model.

III. RESULTS AND DISCUSSION

We first constructed chemical potential diagrams of Cu-In-Se and Cu-Ga-Se systems to determine the range of chemical potentials where CIS and CGS are stable. Relative chemical potentials of Cu, In, Ga, and Se are defined as $\Delta\mu_i = \mu_i - \mu_i^\circ$ ($i =$ Cu, In, Ga, and Se), where μ_i is the chemical potential of atom i and μ_i° is the chemical potential at the standard state, namely Cu (space group $Fm\bar{3}m$), In ($I4/mmm$), Ga ($Cmca$), and Se ($P3_121$). The following competing phases were considered: Cu_2Se ($F\bar{4}3m$), Cu_3Se_2 ($P\bar{4}2_1m$), CuSe ($P6_3/mmc$), $CuSe_2$ ($Pnnm$), Cu_2In ($P6_3mmc$), Cu_9In_4 ($P\bar{4}3m$), In_4Se_3 ($Pnnm$), InSe ($R3m$), In_6Se_7 ($P2_1$), In_2Se_3 ($R3m$ and Cc), $CuIn_5Se_8$ (type D[23] $P\bar{4}$ and $C2$), Cu_9Ga_4 ($P\bar{4}3m$), GaSe ($P6_3/mmc$ and $P\bar{6}m2$), Ga_2Se_3 (Cc), $CuGa_5Se_8$ (type D[23] $P\bar{4}$ and $C2$). Figures 2(a) and 2(c) show the stable phases as a function of the relative chemical potentials for the Cu-In-Se system, and for the Cu-Ga-Se system in Figs. 2(b) and 2(d). These chemical potential diagrams were drawn using the Chesta code.[24] The chemical potential range where CIS and CGS are stable can be described by $\Delta\mu_{Cu}$ and either $\Delta\mu_{In}$ or $\Delta\mu_{Ga}$ because $\Delta\mu_{Cu}$, $\Delta\mu_{In}$ or $\Delta\mu_{Ga}$, and $\Delta\mu_{Se}$ are related by $\Delta\mu_{Cu} + \Delta\mu_{In} + 2\Delta\mu_{Se} = \Delta E_f$ (CIS) and $\Delta\mu_{Cu} + \Delta\mu_{Ga} + 2\Delta\mu_{Se} = \Delta E_f$ (CGS), where ΔE_f (CIS) and ΔE_f (CGS) are the formation energies of CIS and CGS, respectively. The stable phases in the Cu-In-Se system and phase boundaries with CIS are similar to previously reported results with the LDA[3] and a HSE hybrid functional.[25] The $CuGa_5Se_8$ phase does not appear in contrast to a previous report[26] in the Cu-Ga-Se system. This is because the most stable monoclinic phase was considered for Ga_2Se_3 (also for In_2Se_3) in our study, whereas a metastable tetragonal phase was considered in Ref. 26 based on the consideration for In_2Se_3 in Ref. 23.

Figure 3 shows an 11-layer faceted slab model of CIS where the (110) surface is covered by (112) and (11$\bar{2}$) facets. The right half is anion terminated while the left half is cation terminated. Although each facet constitutes a polar surface, the combined surface is stoichiometric and nonpolar, and together should be regarded as a modified or reconstructed surface. The vacuum region between the slabs corresponds to nine layers of CIS or CGS. The electrostatic catastrophe is avoided because there is no net dipole moment in the thickness direction. The use of this model with no net dipole moment is based on the assumption that the net dipole moment, that is, the internal electric field generated by the polar surfaces, should be compensated by a variety of mechanisms such as the formation of reconstructed structures and point defects, adsorption at the surfaces, and/or screening by free careers in metallic substrates. Our model is

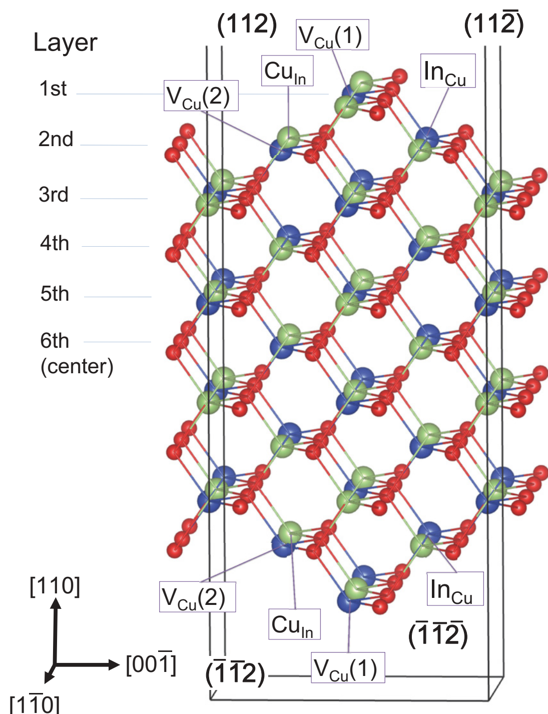

FIG. 3. (Color online) Structure of an 11-layer slab model with facets on the (110) and ($\bar{1}\bar{1}$0) surfaces of CIS. The right half is anion terminated while the left half is cation terminated. The considered point defects are indicated. The blue, green, and red balls denote Cu, In, and Se atoms, respectively.

different from that adopted by Jaffe and Zunger,[3] in which two surfaces are terminated with cation-only and anion-only polar faces, and thus defects and/or carriers inevitably exist at the surface to remove the internal electric field. The concept of the faceted slab model can be a powerful tool for investigating polar surfaces and interfaces. Examples include the {111} polar surfaces and interfaces of zincblende and rocksalt structures, where {111} facets can be made on the nonpolar {110} surface.

Defect formation, namely Cu vacancies and cation antisites, has been reported to lower the surface energies of CIS (112) and (11$\bar{2}$) surfaces.[3] Consequently, we consider a total of nine (110) surface models: The plain (110) surface without facets, and a combination of four cation-terminated facets [pristine, with $V_{Cu}(1)$, $2V_{Cu} = V_{Cu}(1) + V_{Cu}(2)$, and Cu_{In} or Cu_{Ga}] and two anion-terminated facets (pristine and with In_{Cu} or Ga_{Cu}) based on the faceted slab model. Only charge neutral surfaces are considered.

Figures 4(a) and 4(b) show the energies of the most stable surface for CIS and CGS as a function of the relative chemical potentials, respectively. The surface energy for CIS is defined as

$$E_{\mathrm{surface}} = E_{\mathrm{slab}} - E_{\mathrm{bulk}} + \Delta n_{\mathrm{Cu}}\left(\mu^{\circ}_{\mathrm{Cu}} + \Delta\mu_{\mathrm{Cu}}\right) + \Delta n_{\mathrm{In}}\left(\mu^{\circ}_{\mathrm{In}} + \Delta\mu_{\mathrm{In}}\right), \quad (1)$$

where E_{slab} is the total energy of the slab model, E_{bulk} is the energy of bulk CIS with the number of the Se atoms equal to that in the slab model, and Δn_{Cu} and Δn_{In} are the numbers of the Cu and In atoms in the slab that are removed from the corresponding stoichiometric slab. The surface energy of CGS is defined similarly. The values normalized by the surface area are plotted in Figs. 4(a) and 4(b). The chemical potential dependence of the surface energies and most stable configurations is described using $\Delta\mu_{\mathrm{Cu}}$ and $\Delta\mu_{\mathrm{In}}$ or $\Delta\mu_{\mathrm{Ga}}$ only in Fig. 4 as well as in Eq. (1) via the relation $\Delta\mu_{\mathrm{Se}} = [\Delta E_f(\mathrm{CIS}) - \Delta\mu_{\mathrm{Cu}} - \Delta\mu_{\mathrm{In}}]/2$ for CIS or $\Delta\mu_{\mathrm{Se}} = [\Delta E_f(\mathrm{CGS}) - \Delta\mu_{\mathrm{Cu}} - \Delta\mu_{\mathrm{Ga}}]/2$ for CGS. The surface areas are normalized with that of the original (110) surface to allow

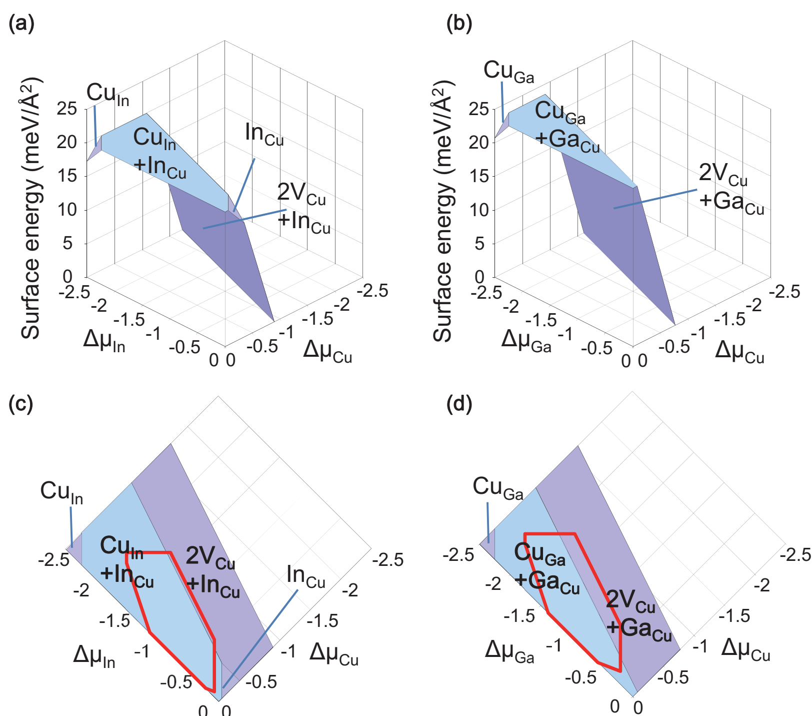

FIG. 4. (Color online) Surface energies for the most stable configurations in (a) CIS and (b) CGS. The most stable configurations with respect to $\Delta\mu_{\mathrm{Cu}}$ and $\Delta\mu_{\mathrm{In}}$ or $\Delta\mu_{\mathrm{Ga}}$ in (c) CIS and (d) CGS. The region where CIS or CGS is stable is enclosed by red lines. Chemical potentials are shown in eV.

direct comparison between the nonfaceted and faceted (110) surfaces. Making (112) and $(11\bar{2})$ facets instead of a (110) surface macroscopically increases the surface area by a factor of approximately 1.227 (Ref. 3), but microscopically the areas of the (112) and $(11\bar{2})$ facets become ill-defined for facet widths at the atomic scale. Figures 4(c) and 4(d) show the most stable surface with respect to chemical potentials of Cu and In or Ga. The areas enclosed in the red lines show the ranges where CIS and CGS are stable, which are also given in Figs. 2(c) and 2(d). There are two stable surfaces for both CIS and CGS, namely surfaces with ($2V_{Cu}$ + In_{Cu}) or ($2V_{Cu}$ + Ga_{Cu}) and (Cu_{In} + In_{Cu}) or (Cu_{Ga} + Ga_{Cu}). The chemical potential range in CIS where ($2V_{Cu}$ + In_{Cu}) is stable is very narrow as shown in Fig. 4(c), whereas the chemical potential range in CGS that stabilizes the ($2V_{Cu}$ + Ga_{Cu}) is wider [Fig. 4(d)].

The plain (110) surface, the faceted surface with no defects, and the faceted surface with Cu_{In} + In_{Cu} defects in CIS (or Cu_{Ga} + Ga_{Cu} in CGS) are stoichiometric; therefore the surface energy does not depend on the chemical potentials. The plain (110) surface has 5.1 meV/Å^2 higher energy than the (Cu_{In} + In_{Cu}) surface in CIS and 1.5 meV/Å^2 higher energy than the (Cu_{Ga} + Ga_{Cu}) surface in CGS and, therefore, is never the lowest energy surface under any chemical potential values. The pristine facets have 11.2 meV/Å^2 higher energy than the (Cu_{In} + In_{Cu}) surface in CIS and 10.2 meV/Å^2 higher energy than the (Cu_{Ga} + Ga_{Cu}) surface in CGS, hence both of these surfaces have higher energy than the corresponding nonfaceted (110) surfaces. Therefore, both CIS and CGS prefer to have faceted surfaces with defects, and epitaxial growth of CIS and CGS is likely to result in a high concentration of defects including vacancies and antisites at surfaces where the type of defect depends on the chemical potentials.

Figure 5 shows the IPs for different slab thicknesses in the two stable surfaces of CIS and CGS. The bulk-based IPs of the ($2V_{Cu}$ + In_{Cu}) and ($2V_{Cu}$ + Ga_{Cu}) surfaces are almost independent of the slab thickness, indicating that the bulklike environment far from the surfaces is well reproduced even in the thinnest slab model with 11 layers. The surface-sensitive IPs decrease with slab thickness and seem to converge to nearly the same values as the bulk-based IPs. Here the difference

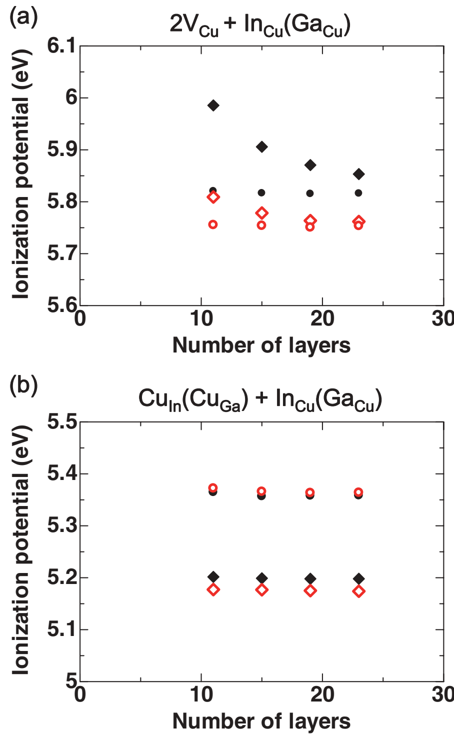

FIG. 5. (Color online) Bulk-based and surface sensitive ionization potentials (IPs) for CIS and CGS for two types of surface defects each as a function of the number of layers in slab models. Red and black symbols indicate IPs for CIS and CGS, respectively. Circles denote bulk-based IPs while diamonds represent surface-sensitive IPs.

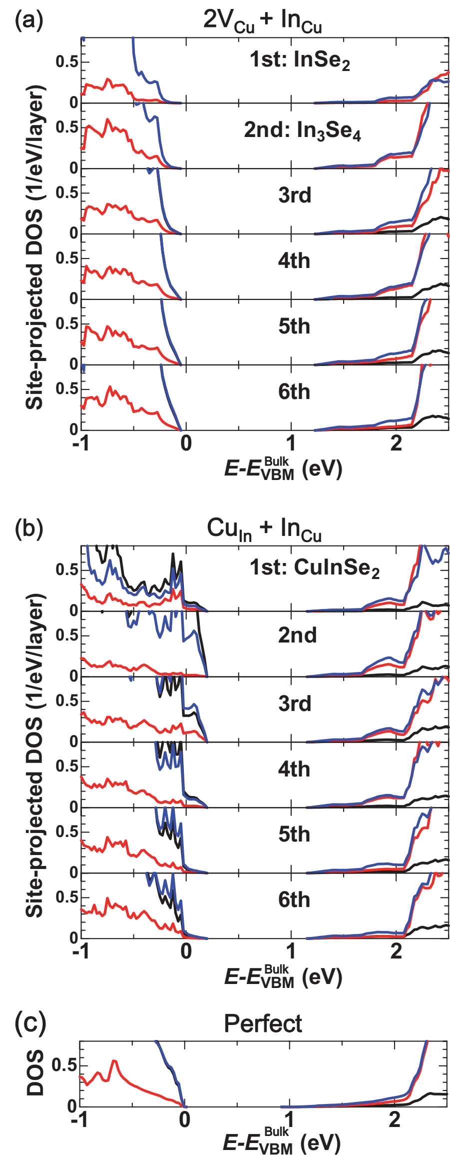

FIG. 6. (Color online) Site projected DOS for the first to sixth layers from the surface in 11-layer slab models of CIS with (a) ($2V_{Cu}$ + In_{Cu}) and (b) (Cu_{In} + In_{Cu}) surfaces and (c) bulk CIS. The bulk VBM is set at zero energy and the surface DOS are aligned with the bulk DOS. The DOS is per $Cu_2In_2Se_4$ layer unless otherwise shown. The black, red, and blue curves denote projected DOS for Cu, In, and Se components, respectively.

TABLE III. Ionization potentials (IPs) of (112) and $(11\bar{2})$ faceted CIS and CGS surfaces with various surface defects and nonfaceted (110) surfaces.[a]

Defects		Surface-sensitive IP (eV)		Bulk-based IP (eV)	
Cation-terminated facets	Anion-terminated facets	CIS	CGS	CIS	CGS
None	*None*	5.58	5.76	5.74	5.82
V_{Cu}	*None*	*	*	5.68	5.93
$2V_{Cu}$	*None*	*	*	5.68	5.66
Cu_{In}/Cu_{Ga}	*None*	*	*	5.61	5.69
None	In_{Cu}/Ga_{Cu}	*	*	5.31	5.34
V_{Cu}	In_{Cu}/Ga_{Cu}	5.36	5.43	5.73	5.82
$2\mathrm{V_{Cu}}$	$\mathrm{In_{Cu}/Ga_{Cu}}$	*	*	5.76	5.82
$\mathrm{Cu_{In}/Cu_{Ga}}$	$\mathrm{In_{Cu}/Ga_{Cu}}$	5.18	5.20	5.37	5.36
(*No facet*)		*	*	5.64	5.70

[a]Italic states indicate unstable surfaces. Surface-sensitive IPs denoted with an asterisk should converge to the same values as the bulk-based IPs because there is no occupied surface state in the band gap.

between the two IPs is inversely proportional to the square of the slab thickness. On the other hand, both IPs of the ($\mathrm{Cu_{In}}$ + $\mathrm{In_{Cu}}$) and ($\mathrm{Cu_{Ga}}$ + $\mathrm{Ga_{Cu}}$) surfaces appear to be independent of the slab thickness. The surface-sensitive IPs are approximately 0.2 eV lower than the bulk-based IPs for both CIS and CGS.

The reason for the different behavior between the ($\mathrm{Cu_{In}}$ + $\mathrm{In_{Cu}}$) and ($\mathrm{Cu_{Ga}}$ + $\mathrm{Ga_{Cu}}$) surfaces and ($2\mathrm{V_{Cu}}$ + $\mathrm{In_{Cu}}$) and ($2\mathrm{V_{Cu}}$ + $\mathrm{Ga_{Cu}}$) surfaces can be understood on the basis of their electronic structures. Figure 6 shows the site-projected density of electronic states (DOS) for the 11-layer slab models of the CIS ($2\mathrm{V_{Cu}}$ + $\mathrm{In_{Cu}}$) and ($\mathrm{Cu_{In}}$ + $\mathrm{In_{Cu}}$) surfaces along with the bulk DOS. The GGA + U internal coordinates were used as in the case of the evaluation of the IPs for consistency. The bulk VBM is chosen as the zero energy, and the surface DOS is aligned with the bulk DOS using the average electrostatic potentials at the three layers at the center of the slab and in the bulk. The DOS near the VBM and CBM for the first [the cusp made by (112) and $(11\bar{2})$ facets] to sixth (center) layers are shown (Fig. 3). There is a striking contrast between the valence bands of the two surfaces. For the ($2\mathrm{V_{Cu}}$ + $\mathrm{In_{Cu}}$) surface shown in Fig. 6(a), no localized surface states are found and the band gap widens near the surface. The shape of the DOS is similar to that of the bulk. Note that the DOS for Cu does not exist at the outmost two layers because there are no Cu atoms in these layers, and is not visible for the third to sixth layers from the surface because the Cu DOS almost overlaps with the Se DOS near the VBM. Furthermore, there is only one In and two Se atoms in the first layer compared to two In and four Se atoms in the third to sixth layers and bulk, and therefore the DOS in the first layer is about half of that in the third to sixth layers and bulk. The change in the surface-sensitive IP [Fig. 5(a)] can be considered to arise from the change in the relative amount of the surface, which prefers to have a wider band gap, to the rest of the slab that prefers the band gap to be equal to the bulk value. As a result, the two IPs are expected to converge to the same value at the infinite thickness limit, which is indeed observed in Fig. 5(a). The bulk-based IP can be used as the single value of the IP in this situation. In contrast, particular electronic states are recognized for the ($\mathrm{Cu_{In}}$ + $\mathrm{In_{Cu}}$) surface shown in Fig. 6(b). The shape of the DOS is clearly different from that of the bulk at the second and third layers that comprise part of the facets (Fig. 3). Occupied surface states, which are mostly localized on the second layer that includes $\mathrm{Cu_{In}}$ and $\mathrm{In_{Cu}}$, distribute up to approximately 0.2 eV above the bulk VBM (zero energy in Fig. 6). On the other hand, the edges of the main structure in the valance DOS at the fifth and sixth layers almost correspond to the bulk VBM. This explains the 0.2 eV difference between the two IPs in Fig. 5(b), showing that the surface-sensitive IP strongly reflects the electronic states at this surface.

Table III summarizes the two IPs obtained using bulk models and slab models composed of 11 layers (12 layers for the unfaceted surface) for the nine surfaces considered in CIS and CGS. Surface-sensitive IPs denoted with an asterisk, such as those for the ($2\mathrm{V_{Cu}}$ + $\mathrm{In_{Cu}}$) and ($2\mathrm{V_{Cu}}$ + $\mathrm{Ga_{Cu}}$) surfaces, are considered to converge to the same values as the bulk-based IPs because there is no occupied surface state in the band gap. The bulk-based IPs of two stable surfaces, namely surfaces of CIS with ($2\mathrm{V_{Cu}}$ + $\mathrm{In_{Cu}}$) and ($\mathrm{Cu_{In}}$ + $\mathrm{In_{Cu}}$) and those of CGS with ($2\mathrm{V_{Cu}}$ + $\mathrm{Ga_{Cu}}$) and ($\mathrm{Cu_{Ga}}$ + $\mathrm{Ga_{Cu}}$), differ by 0.39 eV in CIS and 0.46 eV in CGS, where the Cu-poor surface with $2\mathrm{V_{Cu}}$ has a larger IP (the VBM is lower). The IP differs by less than 0.08 eV when the width of the facets were doubled in CIS and 0.05 eV in CGS, indicating that there is no need to further widen the facets to discuss the difference between the two surfaces with different surface defects. The IPs of the corresponding CIS and CGS surfaces are almost the same within about 0.1 eV except for the $\mathrm{V_{Cu}}$ surface. The ionization potential of a CIS (011) surface has been reported as 5.65 eV by Klein *et al.* through photoelectron spectroscopy measurements for cleaved surfaces of CIS single crystals.[27] Kelvin probe force microscope measurements by Sadewasser *et al.* showed that the work functions of (112) and $(\bar{1}\bar{1}\bar{2})$ surfaces of p-type CGS are 4.87 ± 0.07 and 5.06 ± 0.07 eV for films on ZnSe substrates and 5.30 ± 0.07 and 5.47 ± 0.07 eV for films on Mo/glass substrates.[28] These values are not significantly different from the surface-sensitive and bulk-based IPs of 5.18–5.76 eV for the stable ($2\mathrm{V_{Cu}}$ + $\mathrm{In_{Cu}}$) and ($\mathrm{Cu_{In}}$ + $\mathrm{In_{Cu}}$) CIS surfaces and 5.20–5.82 eV for the stable ($2\mathrm{V_{Cu}}$ + $\mathrm{Ga_{Cu}}$) and ($\mathrm{Cu_{Ga}}$ + $\mathrm{Ga_{Cu}}$) CGS surfaces, although the direct comparison cannot be made because of the difference in the surface structure and the

definition of the measured and calculated quantities. We found that IPs calculated using GGA + U instead of HSE06 ($a = 0.3$) were consistently smaller by about 0.4 to 0.5 eV, thereby underestimating the experimental values. The valence band positions of CIS and CGS are likely to be better described by HSE06 ($a = 0.3$) than GGA + U as well as their band gaps.

IV. CONCLUSIONS

We have investigated the IPs of CIS and CGS based on two definitions using hybrid Hartree-Fock density functional theory calculations. Slab models of the chalcopyrite (110) surface with both (112) and (11$\bar{2}$) facets on each surface of the slab are considered, and chemical potential control can make either a combination of In_{Cu} (Ga_{Cu}) and Cu_{In} (Cu_{Ga}) antisites or a combination of Cu vacancies and Cu_{In} (Cu_{Ga}) antisites stable on the faceted (110) surface. The IPs are evaluated with a definition highly sensitive to and the other less sensitive to localized surface states. The latter varies by 0.4 eV in CIS and 0.5 eV in CGS with the surface structure. The IPs are reduced by 0.2 eV for faceted surfaces with In_{Cu} (Ga_{Cu}) and Cu_{In} (Cu_{Ga}) antisites when the effects of the localized surface states are considered. The values of both IPs are similar between CIS and CGS with a difference of about 0.1 eV for the most stable surface structures.

ACKNOWLEDGMENTS

This work was supported by a Grant-in-Aid for Young Scientists (A) from JSPS and the MEXT Elements Strategy Initiative to Form Core Research Center "Tokodai Institute for Element Strategy (TIES)." Computing resources of ACCMS at Kyoto University were used in this work. The VESTA code[29] was used to draw Fig. 3.

*hinuma.yoyo.2c@kyoto-u.ac.jp

†oba@cms.mtl.kyoto-u.ac.jp

[1] S. Wagner, J. L. Shay, P. Migliorato, and H. M. Kasper, Appl. Phys. Lett. **25**, 434 (1974).

[2] U. Rau and H. W. Schock, Appl. Phys. A **69**, 131 (1999).

[3] J. E. Jaffe and A. Zunger, Phys. Rev. B **64**, 241304 (2001).

[4] S. Siebentritt, N. Papathanasiou, J. Albert, and M. C. Lux-Steiner, Appl. Phys. Lett. **88**, 151919 (2006).

[5] H. Hosono, in *Transparent Electronics from Synthesis to Applications*, edited by A. Facchetti and T. J. Marks (John Wiley and Sons, Chichester, UK, 2010), p. 31.

[6] P. E. Blöchl, Phys. Rev. B **50**, 17953 (1994).

[7] J. Heyd, G. Scuseria, and M. Ernzerhof, J. Chem. Phys. **118**, 8207 (2003).

[8] J. Heyd and G. Scuseria, J. Chem. Phys. **120**, 7274 (2004).

[9] A. V. Krukau, O. A. Vydrov, A. F. Izmaylov, and G. E. Scuseria, J. Chem. Phys. **125**, 224106 (2006).

[10] G. Kresse and J. Hafner, Phys. Rev. B **48**, 13115 (1993).

[11] G. Kresse and J. Furthmüller, Phys. Rev. B **54**, 11169 (1996).

[12] G. Kresse and D. Joubert, Phys. Rev. B **59**, 1758 (1999).

[13] J. Paier, M. Marsman, K. Hummer, G. Kresse, I. C. Gerber, and J. G. Angyan, J. Chem. Phys. **124**, 154709 (2006).

[14] F. Oba, A. Togo, I. Tanaka, J. Paier, and G. Kresse, Phys. Rev. B **77**, 245202 (2008).

[15] A. Alkauskas, P. Broqvist, F. Devynck, and A. Pasquarello, Phys. Rev. Lett. **101**, 106802 (2008).

[16] Y. Kumagai, Y. Soda, F. Oba, A. Seko, and I. Tanaka, Phys. Rev. B **85**, 033203 (2012).

[17] J. Pohl, A. Klein, and K. Albe, Phys. Rev. B **84**, 121201 (2011).

[18] J. P. Perdew, K. Burke, and M. Ernzerhof, Phys. Rev. Lett. **77**, 3865 (1996).

[19] S. L. Dudarev, G. A. Botton, S. Y. Savrasov, C. J. Humphreys, and A. P. Sutton, Phys. Rev. B **57**, 1505 (1998).

[20] A. Walsh and C. R. A. Catlow, J. Mater. Chem. **20**, 10438 (2010).

[21] M. V. Hohmann, P. Ágoston, A. Wachau, T. J. M. Bayer, J. Brötz, K. Albe, and A. Klein, J. Phys.: Condens. Matter **23**, 334203 (2011).

[22] P. G. Moses, M. Miao, Q. Yan, and C. G. Van de Walle, J. Chem. Phys. **134**, 084703 (2011).

[23] S. B. Zhang, S.-H. Wei, A. Zunger, and H. Katayama-Yoshida, Phys. Rev. B **57**, 9642 (1998).

[24] N. Hatada, http://www.aqua.mtl.kyoto-u.ac.jp/chestaEng.html

[25] J. Pohl, T. Unold, and K. Albe, arXiv:1205.2556v1.

[26] C. Persson, Y.-J. Zhao, S. Lany, and A. Zunger, Phys. Rev. B **72**, 035211 (2005).

[27] A. Klein, T. Loher, C. Pettenkofer, and W. Jaegermann, J. Appl. Phys. **80**, 5039 (1996).

[28] S. Sadewasser, T. Glatzel, M. Rusu, A. Jager-Waldau, and M. C. Lux-Steiner, Appl. Phys. Lett. **80**, 2979 (2002).

[29] K. Momma and F. Izumi, J. Appl. Crystallogr. **44**, 1272 (2011).

[30] H. W. Spiess, U. Haeberlen, G. Brandt, A. Räuber, and J. Schneider, Phys. Status Solidi B **62**, 183 (1974).

[31] M. V. Yakushev, F. Luckert, C. Faugeras, A. V. Karotki, A. V. Mudryi, and R. W. Martin, Appl. Phys. Lett. **97**, 152110 (2010).

[32] J. L. Shay, B. Tell, H. M. Kasper, and L. M. Schiavone, Phys. Rev. B **5**, 5003 (1972).